

LoCAtion: Long-time Collaborative Attention Framework for High Dynamic Range Video Reconstruction

Qianyu Zhang, Bolun Zheng*, *Member, IEEE*, Lingyu Zhu, Aiai Huang, Zongpeng Li, *Senior Member, IEEE*, Shiqi Wang, *Senior Member, IEEE*

Abstract—Prevailing High Dynamic Range (HDR) video reconstruction methods are fundamentally trapped in a fragile alignment-and-fusion paradigm. While explicit spatial alignment can successfully recover fine details in controlled environments, it becomes a severe bottleneck in unconstrained dynamic scenes. By forcing rigid alignment across unpredictable motions and varying exposures, these methods inevitably translate registration errors into severe ghosting artifacts and temporal flickering. In this paper, we rethink this conventional prerequisite. Recognizing that explicit alignment is inherently vulnerable to real-world complexities, we propose LoCAtion, a Long-time Collaborative Attention framework that reformulates HDR video generation from a fragile spatial warping task into a robust, alignment-free collaborative feature routing problem. Guided by this new formulation, our architecture explicitly decouples the highly entangled reconstruction task. Rather than struggling to rigidly warp neighboring frames, we anchor the scene on a continuous medium-exposure backbone and utilize collaborative attention to dynamically harvest and inject reliable irradiance cues from unaligned exposures. Furthermore, we introduce a learned global sequence solver. By leveraging bidirectional context and long-range temporal modeling, it propagates corrective signals and structural features across the entire sequence, inherently enforcing whole-video coherence and eliminating jitter. Extensive experiments demonstrate that LoCAtion achieves state-of-the-art visual quality and temporal stability, offering a highly competitive balance between accuracy and computational efficiency.

Index Terms—High Dynamic Range Video Reconstruction, Temporally Coherent, Motion-Aware.

I. INTRODUCTION

HIGH dynamic range (HDR) video acquisition seeks to faithfully capture the luminance of real-world scenes from deep shadows to intense highlights [1]. While specialized hardware sensors [2]–[4] directly expand the dynamic range, they often incur prohibitive costs and lack the flexibility required for widespread deployment. Therefore, computational approaches have become highly practical alternatives to overcome these hardware limitations.

To synthesize HDR videos computationally, combining multiple exposure sequences with low dynamic range has become the mainstream approach. Regardless of whether the capture setup utilizes alternating exposure levels [5], [6] or a continuous medium-exposure stream [7], most existing deep learning methods formulate the core reconstruction task as a

Qianyu Zhang, Bolun Zheng, Aiai Huang, Zongpeng Li are with the School of Automation, Hangzhou Dianzi University, Hangzhou 310018, China (e-mail: qyzhang@hdu.edu.cn; blzheng@hdu.edu.cn; zongpeng@tsinghua.edu.cn). Lingyu Zhu and Shiqi Wang are with the Department of Computer Science, City University of Hong Kong (e-mail: lingyuzhu-c@my.cityu.edu.hk; shiqiwang@cityu.edu.hk)

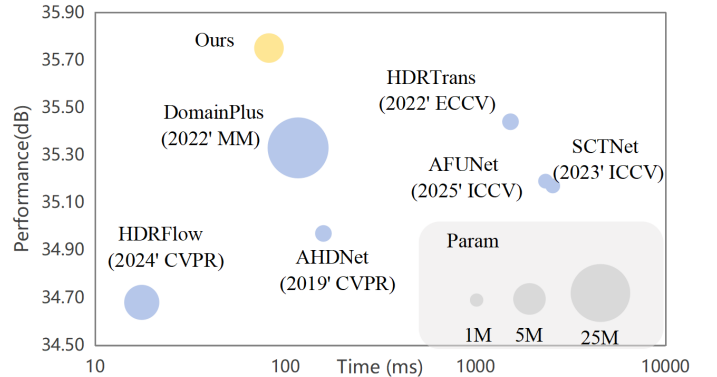


Fig. 1. **Speed-performance trade-off comparison** with recent state-of-the-art HDR methods on the Cinematic Video dataset. Our method achieves state-of-the-art reconstruction quality while maintaining a competitive accuracy-latency trade-off.

frame-centric alignment and fusion pipeline [6], [8], [9]. In this classical formulation, the network typically operates on a local sliding window, explicitly registering adjacent supporting frames to a target reference in the spatial domain, and then fusing them independently to generate each output frame. When evaluated on synthetic datasets or constrained scenarios, this alignment-based strategy often yields highly satisfactory visual results and strong quantitative metrics.

However, although current methods have made significant progress under these ideal conditions, robust reconstruction in complex real-world scenes remains a critical challenge. The conventional alignment and fusion paradigm is fundamentally limited when applied to unpredictable environments, inevitably creating two major bottlenecks in robust HDR video generation: 1). Fragility and computational burden of spatial alignment. In the classical pipeline, successfully reconstructing a single HDR frame rigidly depends on precisely aligning neighboring LDR frames to a reference. Yet, recognizing real-world complexities, this spatial prerequisite is inherently vulnerable. Explicit alignment methods (e.g., optical flow [6]) are highly sensitive to large motions, occlusions, and severe brightness inconsistencies across exposures, directly translating alignment errors into severe ghosting artifacts. Conversely, implicit feature space alignment (e.g., deformable convolution [10] or cross-frame attention [11]) offers better tolerance but comes at a steep computational cost. Specifically, global attention mechanisms incur quadratic complexity in sequence length, rendering them prohibitively expensive for long-term video processing and resource-constrained edge devices. 2). Temporal inconsistency and restricted informa-

tion propagation. Prevailing architectures [8]–[10] typically employ a center-anchored sliding window approach, where each support frame is independently processed and fused with the reference. This isolated processing completely severs the temporal connectivity inherent in videos. It precludes effective message passing between support frames and prevents the network from leveraging retroactive corrections from future observations. Even under fixed-reference settings [7] that nominally provide a temporal anchor, frames are treated as near independent reconstruction units, lacking explicit long-range constraints and whole sequence consistency modeling.

To overcome these limitations, we rethink the essential components required for robust HDR video generation. Recognizing that explicit alignment is inherently vulnerable to real-world complexities, we introduce LoCAtion, a Long-time Collaborative Attention framework. Breaking away from the fragile alignment-fusion pipeline, LoCAtion reformulates HDR generation as an alignment-free collaborative feature routing problem. Anchored on a continuous medium-exposure sequence, our network intelligently coordinates unaligned multi-exposure features and long-range temporal dynamics, naturally dividing the highly entangled reconstruction task into two synergistic stages: Stage 1 (Collaborative Feature Attention): To reliably merge multi-exposure features, this stage replaces explicit spatial warping with motion-aware feature routing in the low-frequency wavelet domain. A Temporal Prior Aggregator transports exposure cues, and a Content-Faithful Fusion module robustly combines them to recover local dynamic range. This approach completely bypasses alignment vulnerabilities and avoids the quadratic computational cost of global attention. Stage 2 (Global Sequence Consistency): Instead of treating temporal consistency as a simple smoothing operation, we introduce a learned sequence-level solver. Utilizing Bidirectional Context Aggregation (BCA) and Long Range Temporal Modeling (LRTM), this stage explicitly propagates corrective signals and structural features back and forth across the entire sequence. This bidirectional propagation enforces whole-video coherence, effectively eliminating structural jitter and visual flicker.

We summarize our core contributions as follows:

- **A new Formulation for Video HDR:** We introduce a fundamental theoretical shift by completely abandoning the fragile spatial alignment process. Instead, we formulate HDR video generation as an alignment-free, long-time collaborative feature routing problem, establishing a robust new foundation for unconstrained dynamic scenes.
- **An Effective Two-Stage Architecture:** We design a highly effective two-stage network. It features a Collaborative Feature Attention stage to reliably extract local dynamic range without motion artifacts, and a Global Sequence Consistency stage to strictly enforce temporal smoothness and eliminate visual flicker.
- **Superior Performance and Efficiency:** Extensive evaluations on both synthetic benchmarks and complex real-world scenarios demonstrate that LoCAtion achieves state-of-the-art visual quality. Crucially, it establishes a highly competitive balance between computational efficiency and temporal stability.

II. RELATED WORK

HDR Image Reconstruction. One of the primary methods for HDR imaging is the combination of multiple LDR images captured at different exposures, a process that mirrors HDR video reconstruction from alternating-exposure LDR frames. Early traditional techniques prioritize aligning input images or rejecting motion regions to prevent ghosting artifacts. Alignment-based methods used optical flow [12] for motion estimation, or employed advanced optimization methods like patch-based energy minimization [13] and luminance optimization [14]. Rejection-based methods detect moving areas and exclude them from the final image, using approaches such as intensity differences [15], weighted variance [16], and graph-cut methods [17], [18]. However, these traditional methods often struggle with handling large motion, real-time processing, and complex scenes, leading to suboptimal performance in many practical applications.

With the advancement of deep learning, neural network-based techniques for HDR image reconstruction have garnered considerable interest and have become the dominant approach in this area. Kalantari *et al.* [19] first applied CNNs to multi-exposure HDR imaging using optical flow for alignment. However, due to the presence of motion and saturated regions in LDR images, traditional optical flow methods often lead to misalignment [20], [21]. To address this, optical flow networks like FlowNet were introduced, and SAFNet [22] refined motion estimation. Despite improvements, long-distance motions remain challenging. The attention mechanism was later integrated for dynamic scene alignment, with methods like AHDRNet [23] and Liu *et al.* [24] introducing multi-scale alignment techniques. Transformer-based approaches, such as HDR-Trans [25] and HyHDRNet [26], further enhanced feature representation and semantic consistency. These HDR image reconstruction techniques serve as the foundation for more complex applications, such as HDR video reconstruction. The transition from static image processing to video reconstruction follows similar principles but introduces additional challenges due to the temporal dimension and potential motion between frames.

HDR Video Reconstruction. Rather than relying on expensive dedicated hardware solutions [4], [27]–[29] for capturing HDR videos, many approaches utilize LDR frames with varying exposure levels to reconstruct HDR content. Kang *et al.* [5] first introduced the alternating exposure paradigm, aligning multi-exposure images at each time step and merging them into a single HDR frame. However, challenges persist in accurately aligning and merging these images. Mangiat *et al.* [30] applied block-based motion estimation with refined motion vectors, later enhancing this method with HDR filtering to eliminate block artifacts [31]. Gryaditskaya *et al.* [32] proposed an adaptive weighting algorithm to minimize motion artifacts, while Li *et al.* [33] introduced a statistical method to avoid exact alignment estimation. Despite these advances, such methods are often time-consuming and prone to visible artifacts.

With the advancement of deep learning, researchers have increasingly focused on learning-based approaches to align and

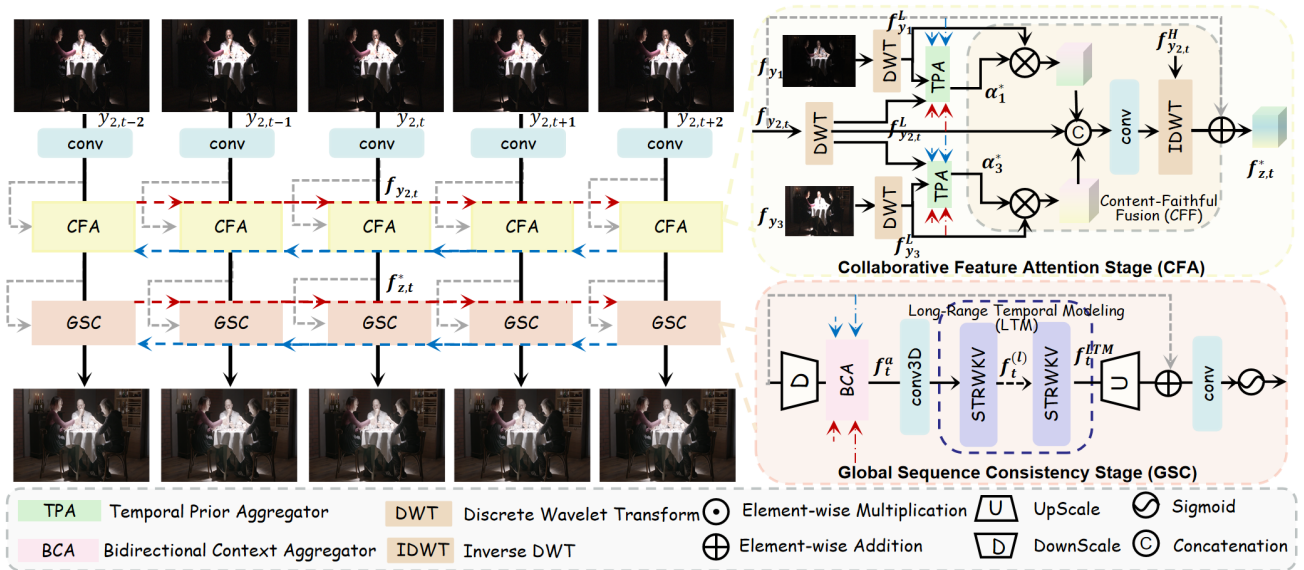


Fig. 2. An overview of the proposed LoCation framework. Our alignment-free architecture naturally decouples the HDR video reconstruction task into two synergistic stages. First, the Collaborative Feature Attention stage operates on a continuous medium-exposure backbone to perform motion-aware collaborative attention, reliably integrating unaligned multi-exposure features to recover local dynamic range. Second, the Global Sequence Consistency stage acts as a sequence-level solver. By leveraging bidirectional context and long-range temporal modeling to explicitly broadcast corrective and structural information, it enforces whole-sequence consistency and effectively eliminates visual flicker.

fuse alternating exposure frames for HDR video reconstruction. Kalantari *et al.* [6] pioneered this direction by aligning alternating exposure frames through optical flow estimation and fusing them in an end-to-end network to generate HDR video. Chen *et al.* [10] introduced a two-stage coarse-to-fine framework, where deformable convolutions enable flexible alignment of complex motions, followed by refined fusion to enhance reconstruction quality. LAN-HDR [11] employed luminance-based attention scores to align adjacent frames with the reference frame and fused features based on these attention weights. HDRFlow [9] developed an efficient flow network with multi-scale large kernels to robustly align frames under large motions, and subsequently fused the aligned features for high-quality HDR output. Cui *et al.* [8] advanced this paradigm by introducing exposure completion through feature interpolation, enabling better alignment across varying exposures and fusing them with a novel decoding architecture.

Unlike existing methods that rely heavily on accurate motion alignment, our approach introduces bidirectional propagation with rejection-driven fusion, offering improved robustness to large motions, occlusions, and exposure variations while maintaining lightweight efficiency.

III. METHODOLOGY

A. Motivation and Problem Formulation

Dynamic HDR video reconstruction is inherently an ill-posed problem, requiring the disentanglement of inter-frame motion from cross-exposure luminance variations. Conventional frame-centric methods struggle with this, often tightly coupling motion estimation with exposure fusion, which inevitably leads to severe ghosting and luminance flicker under complex dynamics.

To fundamentally bypass these bottlenecks, we introduce LoCation, a Long-time Collaborative Attention framework. We adopt the robust capture setup of [7], where a continuous medium-exposure stream $\mathbf{Y} = \{y_{2,t}\}_{t=1}^T$ serves as the stable temporal backbone. To expand the dynamic range without introducing excessive alignment overhead, we utilize a single pair of low and high exposures (y_1, y_3) as dynamic range anchors for a given temporal segment. Rather than rigidly warping these sparse exposure anchors to match the backbone, we recast the reconstruction task as an alignment-free collaborative feature aggregation problem.

Guided by this formulation, our LoCation architecture naturally decouples the reconstruction task into two synergistic objectives: (i) Collaborative Feature Attention (Local Dynamic Range Expansion): We leverage motion-aware collaborative attention to selectively aggregate unaligned multi-exposure features from (y_1, y_3) into the continuous backbone \mathbf{Y} . This stage reliably expands the local dynamic range while strictly avoiding motion-induced ghosting. (ii) Global Sequence Consistency (Long-Range Temporal Modeling): Since local spatial aggregation operates within a restricted temporal receptive field, we introduce a sequence-level solver that bidirectionally propagates corrective context across the entire video, explicitly enforcing long-range temporal coherence.

B. Stage 1: Collaborative Feature Attention

The primary objective of this stage is to perform motion-tolerant exposure fusion. Before detailing the network architecture, it is crucial to clarify a fundamental design choice: why do we discard the explicit alignment step ubiquitous in prior HDR video reconstruction methods.

In traditional alternating-exposure setups, adjacent frames inherently capture different exposure levels. To reconstruct an

HDR frame, existing methods are forced to perform cross-exposure alignment (e.g., optical flow or deformable convolutions) to find motion cues among varying-exposure supports. This process is highly ill-posed: the network struggles to distinguish whether pixel intensity differences arise from actual object motion or merely from exposure variations. Consequently, forced alignment under complex dynamics often collapses, introducing severe warping artifacts and ghosting. The fixed-reference setup fundamentally eliminates this bottleneck. By maintaining a continuous mid-exposure sequence \mathbf{Y} , temporal dynamics can be implicitly tracked along this constant-exposure backbone without the confounding interference of illumination changes. Meanwhile, the low and high exposure anchors (y_1, y_3) are utilized solely to provide global dynamic-range cues, not temporal motion cues. Therefore, instead of performing a fragile explicit spatial warping of the anchors to each backbone frame, we reframe the process as a motion-tolerant feature aggregation. By identifying motion mismatches and learning dynamic reliability maps, we can directly softly gate and inject valid irradiance cues into the backbone, seamlessly bypassing the hazards of explicit alignment.

To realize this robust aggregation while mitigating the interference from high-frequency noise and minor structural discrepancies, we execute this fusion entirely within the low-frequency wavelet domain. Given the input LDR images $[y_1, y_3] \in \mathbb{R}^{3 \times H \times W}$ and the backbone $\mathbf{Y} \in \mathbb{R}^{T \times 3 \times H \times W}$, we project them into a C -channel feature space and apply a Discrete Wavelet Transform (DWT). This yields the half-resolution low-frequency (LL) subband features: the exposure anchors $f_{y_1}^L, f_{y_3}^L \in \mathbb{R}^{C \times \frac{H}{2} \times \frac{W}{2}}$, and the backbone sequence $f_{y_2}^L \in \mathbb{R}^{T \times C \times \frac{H}{2} \times \frac{W}{2}}$.

Temporal Prior Aggregator (TPA). Even without explicit alignment, estimating pixel-wise reliability maps purely from spatial differences between an anchor and a backbone frame remains ambiguous. To robustly identify whether a pixel in the anchor is safe to fuse, we must leverage the temporal context. We propose the Temporal Prior Aggregator (TPA), which leverages bidirectional temporal dynamics from the backbone to construct motion-aware reliability maps α .

Specifically, TPA predicts independent maps α_1 and α_3 for the low and high exposures, respectively. Taking the low-exposure anchor as an example, TPA aggregates forward ($\vec{\mathbf{f}}_t$) and backward ($\overleftarrow{\mathbf{f}}_t$) temporal dependencies:

$$\begin{aligned} \vec{\mathbf{f}}_t &= \mathcal{G}_f([\vec{\mathbf{f}}_{t-1}, f_{y_1}^L, f_{y_2,t}^L]) \\ \overleftarrow{\mathbf{f}}_t &= \mathcal{G}_b([\overleftarrow{\mathbf{f}}_{t+1}, f_{y_1}^L, f_{y_2,t}^L]) \end{aligned} \quad (1)$$

where \mathcal{G}_f and \mathcal{G}_b are convolutional blocks, and $[\cdot, \cdot]$ denotes channel-wise concatenation. The aggregated features are then projected and passed through a sigmoid activation to yield the ambiguity-free reliability map $\alpha_1 \in \mathbb{R}^{C \times \frac{H}{2} \times \frac{W}{2}}$. α_3 is computed analogously.

Content-Faithful Fusion (CFF). Equipped with the robust reliability maps $\alpha = \{\alpha_1, \alpha_3\}$, the complex fusion task simplifies to an attention-guided per-frame aggregation. The CFF module uses α as dynamic soft-gating masks to selectively blend the anchor features into the backbone $f_{y_2}^L$. By

suppressing regions with motion mismatches and emphasizing reliable HDR cues, CFF generates a ghost-free intermediate feature f_Z^L . Finally, the intermediate feature z_t is reconstructed by applying the Inverse DWT to the fused LL band alongside the corresponding high-frequency bands.

C. Stage 2: Global Sequence Consistency

While the Collaborative Feature Attention stage successfully extracts ghost-free representations, this spatial aggregation inherently focuses on local dynamic range recovery. A fundamental flaw of conventional sliding-window architectures is that they stop at this localized processing step, which inevitably leaves the temporal sequence vulnerable to structural jitter and visual flicker. To elevate our locally aggregated features into a globally coherent video, the network must explicitly track long-range structural evolution. Therefore, our second stage shifts the focus from local irradiance injection to whole-sequence temporal consistency.

Instead of treating temporal consistency as a heuristic afterthought (e.g., via simple post-processing losses), our LoCAtion framework elevates it to a first-class objective. Given the intermediate feature sequence $\mathbf{Z} = \{z_1, z_2, \dots, z_T\}$ reconstructed from Stage 1, the goal of this stage is to learn a dense spatio-temporal residual Δ that systematically propagates corrective signals and structural features across the entire video:

$$\mathbf{X} = \mathbf{Z} + \Delta, \quad \text{where}; \Delta = \Psi_{\text{GSC}}(\mathbf{Z}) \quad (2)$$

This residual formulation ensures that the high-fidelity spatial details reliably recovered in Stage 1 are strictly preserved within the intermediate sequence \mathbf{Z} , while global temporal coherence is explicitly enforced through the additive sequence-level update Δ .

To compute Δ efficiently, we first downsample the intermediate sequence \mathbf{Z} using a strided encoder to extract an initial feature representation $\{f_t^{(0)}\}_{t=1}^T$. We then construct a globally informed feature space using two synergistic propagation modules:

Bidirectional Context Aggregation (BCA). To broadcast contextual information back and forth across time, we employ a multi-pass recurrent mechanism. For each pass $k \in \{1, 2\}$, the forward and backward propagated features are formulated as:

$$\begin{aligned} \vec{f}_t^{(k)} &= \mathcal{G}^{\rightarrow,k}([\vec{f}_{t-1}^{(k)}, \mathbf{I}_t^{\rightarrow(k)}]) \\ \overleftarrow{f}_t^{(k)} &= \mathcal{G}^{\leftarrow,k}([\overleftarrow{f}_{t+1}^{(k)}, \mathbf{I}_t^{\leftarrow(k)}]) \end{aligned} \quad (3)$$

where $\mathcal{G}^{\rightarrow,k}$ and $\mathcal{G}^{\leftarrow,k}$ are shared residual blocks. The inputs for the first pass are $\mathbf{I}_t^{\rightarrow(1)} = \mathbf{I}_t^{\leftarrow(1)} = f_t^{(0)}$. To ensure dense information flow and cross-directional awareness, the second pass integrates features from the first: $\mathbf{I}_t^{\rightarrow(2)} = [\overleftarrow{f}_t^{(1)}, f_t^{(0)}]$ and $\mathbf{I}_t^{\leftarrow(2)} = [\vec{f}_t^{(1)}, f_t^{(0)}]$. The thoroughly aggregated features are then concatenated as $f_t^a = [f_t^{(0)}, \vec{f}_t^{(1)}, \overleftarrow{f}_t^{(1)}, \vec{f}_t^{(2)}, \overleftarrow{f}_t^{(2)}]$. **Long-Range Temporal Modeling (LTM).** While BCA excels at aggregating regional temporal context, we introduce a Long-Range Temporal Modeling module to explicitly capture global sequence dependencies. This is achieved by processing

TABLE I

QUANTITATIVE COMPARISONS OF OUR METHOD WITH OTHER STATE-OF-THE-ART METHODS ON THE CINEMATIC VIDEO DATASET. THE TIME IS THE INFERENCE TIME ON THE 1024×1024 RESOLUTION INPUTS. [KEY: **RED** AND **BLUE** INDICATE THE BEST AND THE SECOND-BEST PERFORMANCE. \downarrow (\uparrow) DENOTES THAT SMALLER (LARGER) VALUES, CORRESPONDING TO BETTER PERFORMANCE.]

Methods	STD (\downarrow)	PSNR _T (\uparrow)	SSIM _T (\uparrow)	HDR-VDP-2 (\uparrow)	t-SSIM (\uparrow)	t-PSNR (\uparrow)	AB (\downarrow)	MADB (\downarrow)	Param(M)	Time (ms)
Chen (21' ICCV)	1.91	32.60	0.8702	63.10	0.7128	36.43	50.62	2.75	2.76	167.6
LAN-HDR (23' ICCV)	1.94	33.47	0.8520	62.10	0.7248	36.86	37.71	1.98	7.39	230.7
HDRFlow (24' CVPR)	0.96	34.68	0.8919	62.87	0.7745	37.98	35.08	2.13	5.33	17.6
AHDNet (19' CVPR)	0.82	34.97	0.8593	62.57	0.8137	38.72	32.82	0.96	1.44	158.9
HDRTrans (22' ECCV)	0.83	35.44	0.9044	62.50	0.8275	39.00	32.82	0.99	1.46	1531.3
DomainPlus (22' MM)	0.80	35.33	0.9036	63.22	0.8419	39.11	32.80	0.99	24.78	116.9
SCTNet (23' ICCV)	0.81	35.17	0.9035	62.27	0.8457	39.06	33.61	0.95	0.96	2553.9
AFUNet (25' ICCV)	0.82	35.19	0.9027	62.79	0.8418	39.07	33.18	0.96	1.14	2341.5
Ours	0.71	35.75	0.9051	63.41	0.8572	39.32	32.70	0.94	4.63	82.16

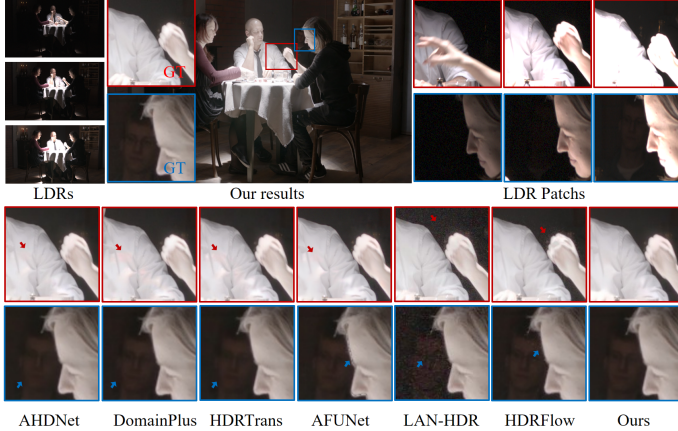


Fig. 3. Visual comparisons on POKER FULLSHOT sequences. Image deghosting methods (e.g., AHDNet, DomainPlus) leave residual ghosting in saturated highlight regions (red box) and blur in dark areas due to insufficient detail recovery (blue box), while video reconstruction methods (e.g., LAN-HDR, HDRFlow) reduce ghosts but introduce noticeable noise and grain. Our method reduces both ghosting and noise, preserving fine structures and contrast in both highlights and shadows. Zoom in for details.

$\{f_t^a\}_{t=1}^T$ through K stacked RWKV blocks [34], [35], which efficiently model long-range interactions with linear complexity:

$$f_t^{(l)} = \text{RWKV}^{(l)}(f_t^{(l-1)}, f_{1:T}^{(l-1)}), \quad l = 1, \dots, K \quad (4)$$

where $f_t^{(0)} = f_t^a$. The final sequence representation f_t^{LTM} is then upsampled and added as the global residual Δ_t to the primary intermediate input z_t , yielding the final temporally coherent HDR sequence \mathbf{X} .

D. Optimization Objective

Let $\tau(\cdot)$ define a logarithmic tone-mapping function $\tau(x) = \frac{\log(1+\kappa x)}{\log(1+\kappa)}$ with $\kappa > 0$. We supervise the network using three tailored loss functions.

First, we enforce spatial fidelity against the ground truth x_t using an L_1 loss in the tone-mapped domain:

$$\mathcal{L}_s = \frac{1}{T} \sum_{t=1}^T \|\tau(\hat{x}_t) - \tau(x_t)\|_1 \quad (5)$$

Second, to explicitly suppress flicker while preserving natural scene motion, we penalize deviations in inter-frame

gradients:

$$\mathcal{L}_t = \frac{1}{T-1} \sum_{t=1}^{T-1} \left\| (\tau(\hat{x}_{t+1}) - \tau(\hat{x}_t)) - (\tau(x_{t+1}) - \tau(x_t)) \right\|_1 \quad (6)$$

Finally, to guarantee that our fusion strictly respects the mid-exposure temporal backbone and prevents the anchors from introducing structural hallucinations, we introduce an Anchor Consistency Loss. Given two intermediate sequences $\mathbf{Z}^{(a)}$ and $\mathbf{Z}^{(b)}$ generated from the same backbone \mathbf{Y} but different anchor pairs, we enforce their structural alignment:

$$\mathcal{L}_Z = \frac{1}{T} \sum_{t=1}^T \left\| z_t^{(a)} - z_t^{(b)} \right\|_1 \quad (7)$$

The overall training objective is the weighted sum of these terms:

$$\mathcal{L}_{\text{total}} = \mathcal{L}_s + \lambda_t \mathcal{L}_t + \lambda_Z \mathcal{L}_Z \quad (8)$$

IV. EXPERIMENTS

A. Experiment Settings

Training Details. We implement our model in PyTorch and train it on an NVIDIA RTX 4090 GPU. Optimization is performed using Adam [36] with an initial learning rate of 10^{-4} , which is decayed until it reaches 10^{-6} . During training, both LDR inputs and their corresponding HDR targets are randomly cropped into 256×256 patches, with a batch size of 4. Random rotations are applied for data augmentation to mitigate overfitting.

Datasets. Following [9]–[11], we construct synthetic training data using the Vimeo-90K septuplet dataset [37]. Since Vimeo-90K is not specifically designed for HDR video reconstruction, we convert the original frames into LDR sequences with alternating exposures and a dual-stream paradigm, following [7] to ensure a fair comparison with previous approaches. For evaluation, due to the limited availability of public HDR video benchmarks, two synthetic sequences (POKER FULLSHOT and CAROUSEL FIREWORKS) from the Cinematic Video dataset are used. Additionally, the real-captured dataset (which consists of 22 different scenes, each containing over 200 frames) [7] is employed for no-reference and qualitative evaluation, due to the lack of ground-truth HDR frames.

Evaluation metrics. We adopt $PSNR_T$, $SSIM_T$, and HDR-VDP-2 [38] as our evaluation metrics. Both $PSNR_T$ and



Fig. 4. Visual comparisons on CAROUSEL FIREWORKS sequences. In fast-motion scenes, video reconstruction baselines (e.g., LAN-HDR/HDRFlow) often break down, exhibiting motion tearing. Image dehazing approaches (e.g., AHRNet, DomainPlus) tend to leave color fringing and halos around moving light trails. Our LoCAtion better handles rapid motion, markedly suppressing ghosting and color fringing.



Fig. 5. Visual comparisons on public real-world videos.

TABLE II
QUANTITATIVE COMPARISONS OF OUR METHOD WITH OTHER STATE-OF-THE-ART METHODS ON THE PUBLIC REAL-CAPTURED VIDEO DATASETS.

Method	LSD (\downarrow)	t-SSIM (\uparrow)	t-PSNR (\uparrow)
DeepHDRVideo(ICCV'21) [10]	14.0	0.7092	19.55
LAN-HDR(ICCV'23) [11]	13.1	0.6527	20.26
HDRFlow(CVPR'24) [9]	11.9	0.7591	20.33
AHDNet(CVPR'19) [23]	1.7	0.8765	29.05
HDR-Trans(ECCV'22) [25]	1.7	0.8729	28.98
DomainPlus(MM'22) [40]	2.5	0.8626	27.10
SCTNet(ICCV'23) [39]	1.8	0.8790 29.06	
AFUNet(ICCV'25) [41]	1.7	0.8776	29.02
Ours	1.6	0.8806	29.12

$SSIM_T$ are computed in the μ -law tonemapped domain [19], consistent with most existing studies. To provide a more comprehensive assessment of video quality, we further introduce temporal-PSNR (t-PSNR), temporal-SSIM (t-SSIM), and the average brightness variation metric AB, mean absolute difference of brightness (MADB), and standard deviation of frame-wise quality metrics (STD) to evaluate the structural stability along the temporal dimension and luminance fluctuations in video sequences, respectively.

Baselines. Our method is evaluated against state-of-the-art video-based HDR reconstruction approaches, including HDRFlow [9], LAN-HDR [11], and DeepHDRVideo [10]. To assess dehazing performance, we further include representative image-based HDR dehazing models such as AHDR [23], HDR-Transformer [25], SCTNet [39], DomainPlus [40], and AFUNet [41]. For fairness, methods relying on few-shot or unsupervised paradigms are excluded, as they are not tailored for supervised multi-exposure HDR video reconstruction.

B. HDR Video Experimental Results

Quantitative Comparisons. Table I summarizes the quantitative results on the Cinematic Video dataset. Our method consistently outperforms all competing approaches across spatial, temporal, and stability metrics. It achieves gains of +0.31 dB in $PSNR_T$ and +0.0007 in $SSIM_T$ over the second best method, and further improves temporal fidelity with +0.21 dB in t -PSNR and +0.0115 in t -SSIM. Moreover, it produces the

most stable reconstruction, reducing temporal fluctuation by 11.25% relative to the next best, demonstrating stronger frame-to-frame consistency.

Qualitative Comparisons. Fig. 3 and 4 present visual comparisons under two challenging scenarios: overexposed highlights and fast motion. In Fig. 3 (POKER FULLSHOT), image-based dehazing methods (e.g., AHDRNet, DomainPlus) leave noticeable ghosts in saturated regions and blur in darker areas, while video-based methods such as LAN-HDR and HDRFlow suppress ghosts but introduce noise and grain. In contrast, our approach removes both ghosting and noise, and better preserves fine details and contrast in highlight and shadow regions. In Fig. 4 (CAROUSEL FIREWORKS), video methods exhibit alignment artifacts around fast-moving light trails, whereas image-based dehazing models produce color halos and residual ghosts along motion boundaries. Our method handles rapid motion more robustly, yielding cleaner light trails and sharper structures with fewer artifacts.

C. Real HDR Video Experimental Results

To assess generalization, we evaluate our approach on public real world videos. Table II reports the quantitative results, and Fig. 5 provides visual comparisons on individual frames. To better analyze temporal behavior, we further visualize consecutive frames in Fig. 6 (challenging daytime scenes with high contrast white walls and bright skies) and Fig. 7 (nighttime scenes with extremely bright lights). Since ground truth HDR frames are unavailable, we follow prior work [7] and use temporal PSNR, temporal SSIM, and the luminance standard deviation (LSD) to measure temporal consistency.

Existing alternating exposure video reconstruction methods exhibit clear limitations on real sequences. Because their reference frames typically change over time, this exposure swapping introduces noticeable global brightness jumps along the time axis. Furthermore, models trained predominantly on the synthetic Vimeo 90K dataset suffer from severe domain shift when applied to real captured sequences. Combined with imperfect motion estimation, these methods leave residual ghosting around moving objects, especially under large motion or partial occlusion. Both effects amplify temporal instabilities, leading to lower temporal PSNR, lower temporal SSIM, and higher LSD.



Fig. 6. Outdoor daytime scene with high-contrast regions. Traditional image-based HDR deghosting methods struggle with visible ghosting across consecutive frames due to the lack of temporal information, leading to artifacts in high-contrast regions. Video-based HDR reconstruction methods lead to clear brightness jumps along the time axis.

Conversely, image-based deghosting methods avoid global brightness flicker by utilizing a fixed medium exposure reference. However, because they operate on each multi-exposure stack independently without temporal propagation or motion reasoning, they cannot distinguish whether a local input misalignment is caused by true content missing due to saturation or by undesirable motion. As a result, details fluctuate across frames, and ghosting artifacts are inevitably preserved in high contrast regions, yielding suboptimal temporal metrics.

In contrast, our method achieves the highest average temporal PSNR and temporal SSIM, alongside the lowest LSD across all real world sequences. By maintaining a stable medium exposure backbone and utilizing our fusion and propagation framework, we elegantly overcome the limitations of previous baselines. Visually, our approach jointly suppresses ghosting and preserves motion consistent details, resulting in highly consistent brightness over time and a marked reduction in artifacts around moving objects.

D. Analysis of Exposure Paradigms

Limitations of alternating exposure sequences. Alternating exposure based HDR video reconstruction methods take an interleaved sequence of short and long exposure LDR frames as input. They attempt to reconstruct an HDR sequence by repeatedly changing the reference frame over time. We observe that, both on synthetic benchmarks (Fig. 8) and in real scenes (Fig. 6 and Fig. 7), this design inevitably leads to large quality fluctuations across frames. As illustrated in Fig. 8(a), existing

synthetic pipelines [8]–[11] typically inject different noise levels into different exposures when generating alternating sequences. When a method reconstructs each frame using a time-varying reference, the reconstruction quality naturally becomes highly sensitive to the chosen reference exposure and its specific noise level, leading to visible temporal instability.

This problem becomes even more severe in real world data. In practice, sensor noise is much more complex than the simple independent and identically distributed noise models used in synthetic datasets, and the exposure pattern of real cameras does not exactly match the synthetic alternating pattern. This domain gap means that methods trained purely on synthetically generated alternating exposure data tend to exhibit strong brightness flicker and unstable contrast when applied to real captured videos. In our experiments on real scenes (see more video demos on our project page), alternating exposure methods often show noticeable frame-to-frame changes in global luminance, alongside local intensity popping in high contrast regions such as light sources and deep shadows.

Advantages of our temporal propagation paradigm. While recent capture setups [7] provide a continuous medium exposure stream to mitigate global flicker, the algorithmic challenge of propagating sparse dynamic range cues across this temporal backbone remains entirely unresolved. Instead of treating these frames as isolated reconstruction targets, we uniquely leverage this stable sequence as a temporal canvas for our attention-guided spatial aggregation and global sequence consistency framework.

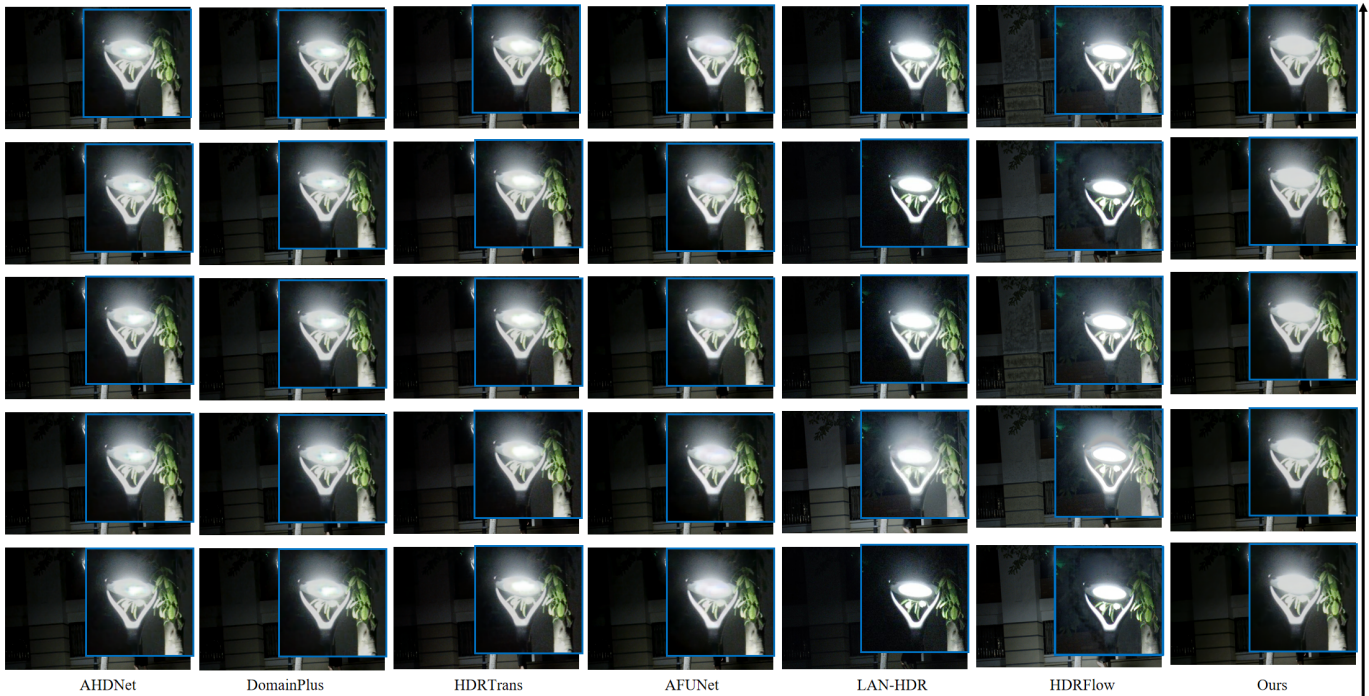


Fig. 7. Nighttime scene with extremely high dynamic range, including bright lights and dark backgrounds.

We provide a single low and high exposure pair strictly at an anchor frame, fundamentally shifting the algorithmic burden from isolated frame-wise alignment to sequence-level information routing. Because the medium exposure backbone possesses highly consistent structural and noise statistics, it serves as an ideal carrier for temporal propagation. Rather than independently fusing multi-exposure stacks at every timestamp like previous methods, our network intelligently extracts extreme luminance details at the anchor and continuously propagates them along the stable backbone. This design elegantly decouples local dynamic range harvesting from global temporal modeling.

Qualitative and quantitative results demonstrate that our specific propagation mechanism dramatically outperforms existing temporal methods. Our reconstructions exhibit highly stable brightness and contrast over time, presenting virtually no ghosting or noise artifacts in both synthetic and real

scenes. Furthermore, we captured custom video sequences and varying exposure images using a commercial smartphone to evaluate our method in the wild, yielding highly robust results (available on our project page).

E. Ablation study

We conduct ablations to answer three questions: (i) *Anchor sufficiency*: is pairing a short group of medium exposure frames with a single low and high anchor adequate, and how sensitive is performance to the sliding window length and the anchor injection density? (ii) *Fusion design*: how does our fusion compare with mainstream alignment schemes (flow-based warping [6], attention [23], cross-attention (CA) [11]), and what are the contributions of our internal choices (TPA reliability maps, LL-domain fusion) to accuracy and ghosting robustness? (iii) *Temporal refinement*: how do BCA and the LTM module affect frame-to-frame consistency?

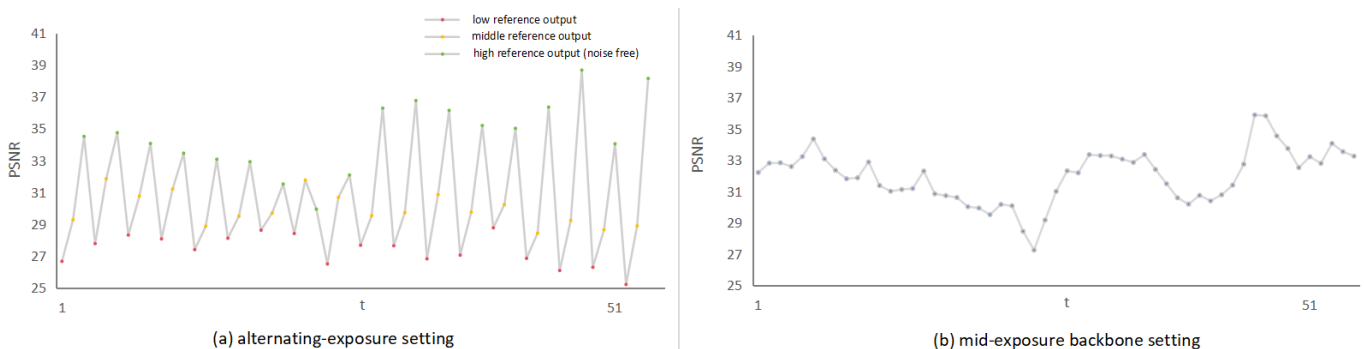


Fig. 8. Illustration of the limitations of alternating-exposure HDR video reconstruction. (a) shows the quality fluctuations of the carousel fireworks scene across frames with the existing alternating-exposure method, (b) demonstrates the temporal stability of our method.

TABLE III
EFFECT OF MID-EXPOSURE SEQUENCE LENGTH T ON ANCHOR SUFFICIENCY AND TEMPORAL STABILITY.

Model	STD (\downarrow)	$PSNR_T$ (\uparrow)	$SSIM_T$ (\uparrow)	AB (\downarrow)
$T = 1$	0.78	35.31	0.9012	32.95
$T = 5$ (Ours)	0.71	35.75	0.9051	32.70
$T = 7$	0.59	35.81	0.9107	22.28
$T = 10$	0.62	35.73	0.9096	24.22
$T = 15$	0.61	35.66	0.9115	8.32
$T = 20$	0.64	35.57	0.9125	4.59

Anchor sufficiency. 1) The impact of medium exposure sequence length T . Our method adopts a unique input configuration where a short medium exposure sequence is paired with a single exposure anchor pair. We first validate this design by varying the sliding window length T of the medium exposure backbone, as summarized in Table V. This length T fundamentally controls how much temporal context is available for propagation away from the anchor, and how far the information from the low and high pair must be transported. When $T = 1$, the model degenerates to a conventional frame-wise multi-exposure fusion setting, where each output relies solely on its local anchors and the effective anchor switches at every frame. This leads to clear degradation in both temporal stability and reconstruction quality, indicating that per-frame anchor switching may be harmful. Expanding the medium exposure sequence to $T = 5$ yields substantial improvements, showing that a single anchor pair shared across a short temporal window is sufficient to recover the dynamic range when combined with temporal propagation.

However, further increasing T enforces the same anchor pair over a longer temporal range. We provide additional qualitative comparisons to dissect this phenomenon in Fig. 10, where we fix all other settings and only vary T . When the temporal distance between a frame and the anchor becomes too large, the reconstruction relies on many propagation steps, which tend to lead to overly smoothed details and a loss of fine spatial features. Consequently, temporal fluctuations are reduced, but reconstruction fidelity is noticeably degraded. Considering the trade-off between reconstruction quality and memory footprint, we set $T = 5$ in all other experiments, while noting that a larger T can be used in high-resource settings to further improve performance.

2) The impact of the number of low and high pairs. Independent of the sliding window size, we investigate how many low and high-exposure pairs are required within each five frame medium-exposure window. In the 1-1 setting, every medium-exposure frame is accompanied by its own low and high-exposure pair. In contrast, our 5-1 configuration uses one low and high pair to support an entire 5-frame window. We further test 10-1, fifteen to one, twenty to one, and 55-1, where a single low and high pair is reused across increasingly longer temporal spans. As shown in our supplementary evaluation regarding anchor density, our 5-1 design achieves the best balance between temporal stability and reconstruction quality. Using a single pair for too short intervals (the 1-1 setting) or too long intervals (from 10-1 up to 55-1) leads to either insufficient temporal context or degraded stability.

Fusion design. Table IV (rows 6-9) and Fig. 9 compare

TABLE IV
ABLATION STUDIES OF THE NETWORK COMPONENTS.

Model	STD (\downarrow)	$PSNR_T$ (\uparrow)	$SSIM_T$ (\uparrow)	AB (\downarrow)	Param	Times
w/o DWT	0.74	35.67	0.9048	32.79	4.50	220.8
w/o $PTPA$	0.75	35.44	0.9004	32.80	3.78	61.3
w/o $RBCA$	0.78	35.16	0.8969	32.80	2.64	80.2
w/o $RLTM$	0.73	35.51	0.9021	32.74	4.71	73.0
$align_{flow}$	1.02	34.76	0.8774	33.76	4.17	153.2
$align_{attention}$	0.80	35.39	0.9016	32.81	3.64	77.2
$align_{CA}$	0.74	35.53	0.9051	32.81	2.45	267.4
Ours	0.71	35.75	0.9051	32.70	4.63	82.2



Fig. 9. Visual comparisons of ablation on different alignment methods. The first stage of our network is replaced with several existing alignment techniques

several fusion strategies under identical training settings. The optical-flow baseline is highly brittle: its performance depends on accurate flow, and estimation errors lead to misalignment and visible ghosting, resulting in a clear quality drop. Replacing flow with local attention or global cross-attention enables feature correlation, but these schemes still lack explicit temporal modeling and constraints, leaving residual ghosts in saturated or fast-moving regions. Moreover, both flow and global attention incur the highest computational latency. In contrast, our fusion module leverages temporal context to refine the reliability maps and suppress unreliable cross-exposure matches, achieving higher accuracy while maintaining a runtime comparable to local attention and substantially lower than flow or global attention.

From rows 2-3, performing fusion in the LL wavelet band effectively reduces computation and latency while maintaining accuracy, as both correspondence and aggregation operate at half resolution. Furthermore, removing the TPA module leads to a notable degradation: without motion-aware reliability guidance, the fusion becomes purely per-frame and tends to over-trust the anchors in saturated or fast-moving regions, resulting in incorrect gating, residual ghosting, and larger temporal fluctuations.

To visually understand this critical effect, we compare the Stage 1 features with and without TPA in Fig. 11. Intuitively, by seeing how structures move over time in the medium exposure sequence, TPA can better decide whether a local mismatch between exposures is caused by true content that should be preserved or by undesired ghosting that should be suppressed. Without TPA, the features around moving regions (e.g., the hand) tend to contain duplicated or smeared structures, reflecting uncertainty about which exposure to trust. With TPA enabled, the corresponding feature responses become significantly more compact and coherent along the motion trajectory, allowing the estimated alpha map to successfully downweight misaligned observations.

Temporal refinement. Table IV (rows 4-5) shows that removing BCA results in notably temporal fluctuations and a



Fig. 10. Ablation study on the impact of mid-exposure sequence length T . Larger T leads to over-smoothed details and a loss of fine spatial features.

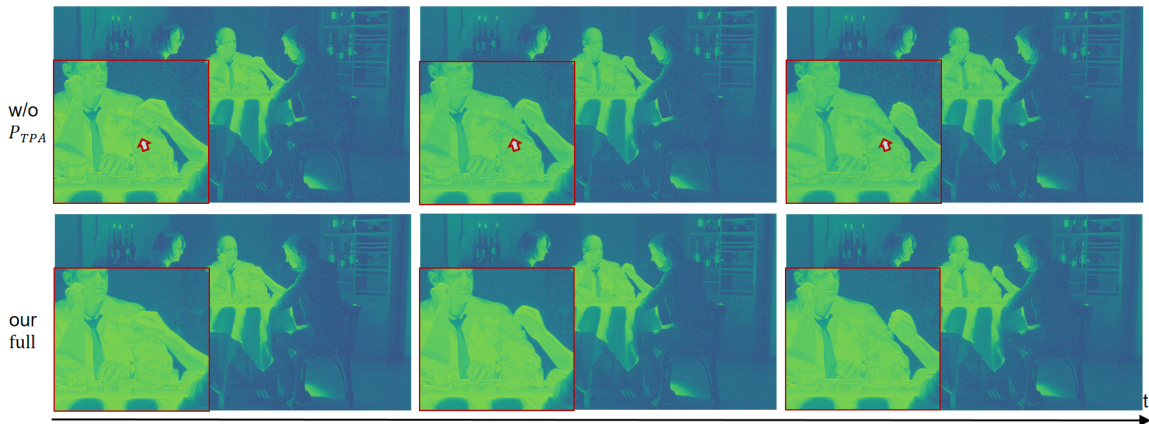


Fig. 11. Ablation study on the impact of Temporal Prior Aggregator (TPA). Without TPA, the features around moving regions (e.g., the hand) tend to exhibit ghosting and duplication due to uncertainty in choosing the correct exposure. This leads to noticeable artifacts in the final HDR output. With TPA, the motion of the hand is reconstructed with less ghosting.

TABLE V
THE IMPACT OF THE NUMBER OF LOW/HIGH PAIRS.

Model	STD (\downarrow)	PSNR R_T (\uparrow)	SSIM T (\uparrow)	AB (\downarrow)
1-1	0.94	35.51	0.9024	32.91
5-1 (Ours)	0.71	35.75	0.9051	32.70
10-1	1.23	36.02	0.9115	32.90
15-1	1.18	35.91	0.9100	32.94
20-1	1.16	35.71	0.9060	32.94
55-1	0.90	35.47	0.9038	32.31

clear drop in accuracy, indicating that BCA provides essential temporal propagation for stabilizing the fusion outputs. The LTM module further complements BCA by modeling long-range dependencies through a lightweight global mechanism. Replacing LTM with a standard residual block slightly improves throughput (73.0 ms), but reduces accuracy.

V. CONCLUSION

In this work, we revisit HDR video reconstruction through a fusion-propagation lens and present a principled MAP-driven formulation that decouples spatial fusion from temporal regularization. Building upon this perspective, we proposed PENet, a two-stage propagation-enhanced framework tailored for reliable and efficient HDR sequence reconstruction. Concretely, we decompose reconstruction into two learnable stages: (i) Joint Spatio-Temporal Fusion, which operates in the wavelet LL band and combines a Temporal Prior Aggregator (TPA) with a Content-Faithful Fusion (CFF) head to inject reliable cross-exposure cues on a fixed mid-exposure backbone; and (ii) Recurrent Temporal Refinement, which uses Bidirectional Context Aggregation (BCA) and Long-Range Temporal Modeling (LTM) as a learned proximal step to enforce sequence-level consistency and suppress flicker. Comprehensive experiments across synthetic and real-world datasets verify that

PENet achieves state-of-the-art reconstruction quality and temporal stability, while maintaining competitive efficiency.

REFERENCES

- [1] P. E. Debevec and J. Malik, "Recovering high dynamic range radiance maps from photographs," in *ACM SIGGRAPH 2008 classes*, 2008, pp. 1–10.
- [2] J. Kronander, S. Gustavson, G. Bonnet, A. Ynnerman, and J. Unger, "A unified framework for multi-sensor hdr video reconstruction," *Signal Processing: Image Communication*, vol. 29, no. 2, pp. 203–215, 2014.
- [3] Y. Jiang, I. Choi, J. Jiang, and J. Gu, "Hdr video reconstruction with tri-exposure quad-bayer sensors," *arXiv preprint arXiv:2103.10982*, 2021.
- [4] J. Han, C. Zhou, P. Duan, Y. Tang, C. Xu, C. Xu, T. Huang, and B. Shi, "Neuromorphic camera guided high dynamic range imaging," in *Proceedings of the IEEE/CVF Conference on Computer Vision and Pattern Recognition*, 2020, pp. 1730–1739.
- [5] S. B. Kang, M. Uyttendaele, S. Winder, and R. Szeliski, "High dynamic range video," *ACM Transactions on Graphics (TOG)*, vol. 22, no. 3, pp. 319–325, 2003.
- [6] N. K. Kalantari and R. Ramamoorthi, "Deep hdr video from sequences with alternating exposures," in *Computer graphics forum*, vol. 38, no. 2. Wiley Online Library, 2019, pp. 193–205.
- [7] Q. Zhang, B. Zheng, L. Zhu, H. Pan, Z. Zhu, Z. Li, and S. Wang, "Capturing stable hdr videos using a dual-camera system," *arXiv preprint arXiv:2507.06593*, 2025.
- [8] J. Cui, W. Jiang, Z. Peng, Z. Pan, and Z. Cao, "Exposure completing for temporally consistent neural high dynamic range video rendering," in *Proceedings of the 32nd ACM International Conference on Multimedia*, 2024, pp. 10027–10035.
- [9] G. Xu, Y. Wang, J. Gu, T. Xue, and X. Yang, "Hdrflow: Real-time hdr video reconstruction with large motions," in *Proceedings of the IEEE/CVF Conference on Computer Vision and Pattern Recognition*, 2024, pp. 24851–24860.
- [10] G. Chen, C. Chen, S. Guo, Z. Liang, K.-Y. K. Wong, and L. Zhang, "Hdr video reconstruction: A coarse-to-fine network and a real-world benchmark dataset," in *Proceedings of the IEEE/CVF international conference on computer vision*, 2021, pp. 2502–2511.
- [11] H. Chung and N. I. Cho, "Lan-hdr: Luminance-based alignment network for high dynamic range video reconstruction," in *Proceedings of the IEEE/CVF International Conference on Computer Vision*, 2023, pp. 12760–12769.
- [12] L. Bogoni, "Extending dynamic range of monochrome and color images through fusion," in *Proceedings 15th International Conference on Pattern Recognition. ICPR-2000*, vol. 3. IEEE, 2000, pp. 7–12.
- [13] P. Sen, N. K. Kalantari, M. Yaesoubi, S. Darabi, D. B. Goldman, and E. Shechtman, "Robust patch-based hdr reconstruction of dynamic scenes," *ACM Trans. Graph.*, vol. 31, no. 6, pp. 203–1, 2012.
- [14] J. Hu, O. Gallo, K. Pulli, and X. Sun, "Hdr deghosting: How to deal with saturation?" in *Proceedings of the IEEE Conference on Computer Vision and Pattern Recognition*, 2013, pp. 1163–1170.
- [15] T. Grosch *et al.*, "Fast and robust high dynamic range image generation with camera and object movement," *Vision, Modeling and Visualization, RWTH Aachen*, vol. 277284, no. 3, p. 2, 2006.
- [16] K. Jacobs, C. Loscos, and G. Ward, "Automatic high-dynamic range image generation for dynamic scenes," *IEEE Computer Graphics and Applications*, vol. 28, no. 2, pp. 84–93, 2008.
- [17] Y. S. Heo, K. M. Lee, S. U. Lee, Y. Moon, and J. Cha, "Ghost-free high dynamic range imaging," in *Asian Conference on Computer Vision*. Springer, 2010, pp. 486–500.
- [18] W. Zhang and W.-K. Cham, "Gradient-directed multiexposure composition," *IEEE Transactions on Image Processing*, vol. 21, no. 4, pp. 2318–2323, 2011.
- [19] N. K. Kalantari, R. Ramamoorthi *et al.*, "Deep high dynamic range imaging of dynamic scenes," *ACM Trans. Graph.*, vol. 36, no. 4, pp. 144–1, 2017.
- [20] F. Peng, M. Zhang, S. Lai, H. Tan, and S. Yan, "Deep hdr reconstruction of dynamic scenes," in *2018 IEEE 3rd International Conference on Image, Vision and Computing (ICIVC)*. IEEE, 2018, pp. 347–351.
- [21] K. R. Prabhakar, R. Arora, A. Swaminathan, K. P. Singh, and R. V. Babu, "A fast, scalable, and reliable deghosting method for extreme exposure fusion," in *2019 IEEE International Conference on Computational Photography (ICCP)*. IEEE, 2019, pp. 1–8.
- [22] L. Kong, B. Li, Y. Xiong, H. Zhang, H. Gu, and J. Chen, "Safnet: Selective alignment fusion network for efficient hdr imaging," in *European Conference on Computer Vision*. Springer, 2024, pp. 256–273.
- [23] Q. Yan, D. Gong, Q. Shi, A. v. d. Hengel, C. Shen, I. Reid, and Y. Zhang, "Attention-guided network for ghost-free high dynamic range imaging," in *Proceedings of the IEEE/CVF Conference on Computer Vision and Pattern Recognition*, 2019, pp. 1751–1760.
- [24] Z. Liu, W. Lin, X. Li, Q. Rao, T. Jiang, M. Han, H. Fan, J. Sun, and S. Liu, "Adnet: Attention-guided deformable convolutional network for high dynamic range imaging," in *Proceedings of the IEEE/CVF Conference on Computer Vision and Pattern Recognition*, 2021, pp. 463–470.
- [25] Z. Liu, Y. Wang, B. Zeng, and S. Liu, "Ghost-free high dynamic range imaging with context-aware transformer," in *European Conference on Computer Vision*. Springer, 2022, pp. 344–360.
- [26] Q. Yan, W. Chen, S. Zhang, Y. Zhu, J. Sun, and Y. Zhang, "A unified hdr imaging method with pixel and patch level," in *Proceedings of the IEEE/CVF Conference on Computer Vision and Pattern Recognition*, 2023, pp. 22211–22220.
- [27] S. K. Nayar and T. Mitsunaga, "High dynamic range imaging: Spatially varying pixel exposures," in *Proceedings IEEE Conference on Computer Vision and Pattern Recognition. CVPR 2000 (Cat. No. PR00662)*, vol. 1. IEEE, 2000, pp. 472–479.
- [28] I. Choi, S.-H. Baek, and M. H. Kim, "Reconstructing interlaced high-dynamic-range video using joint learning," *IEEE Transactions on Image Processing*, vol. 26, no. 11, pp. 5353–5366, 2017.
- [29] H. Zhao, B. Shi, C. Fernandez-Cull, S.-K. Yeung, and R. Raskar, "Unbounded high dynamic range photography using a modulo camera," in *2015 IEEE International Conference on Computational Photography (ICCP)*. IEEE, 2015, pp. 1–10.
- [30] S. Mangiat and J. Gibson, "High dynamic range video with ghost removal," in *Applications of digital image processing XXXIII*, vol. 7798. SPIE, 2010, pp. 307–314.
- [31] —, "Spatially adaptive filtering for registration artifact removal in hdr video," in *2011 18th IEEE International Conference on Image Processing*. IEEE, 2011, pp. 1317–1320.
- [32] Y. Gryaditskaya, T. Pouli, E. Reinhard, K. Myszkowski, and H.-P. Seidel, "Motion aware exposure bracketing for hdr video," in *Computer Graphics Forum*, vol. 34, no. 4. Wiley Online Library, 2015, pp. 119–130.
- [33] Y. Li, C. Lee, and V. Monga, "A maximum a posteriori estimation framework for robust high dynamic range video synthesis," *IEEE Transactions on Image Processing*, vol. 26, no. 3, pp. 1143–1157, 2016.
- [34] B. Peng, E. Alcaide, Q. Anthony, A. Albalak, S. Arcadinho, S. Biderman, H. Cao, X. Cheng, M. Chung, M. Grella *et al.*, "Rwkv: Reinventing rns for the transformer era," *arXiv preprint arXiv:2305.13048*, 2023.
- [35] Y. Duan, W. Wang, Z. Chen, X. Zhu, L. Lu, T. Lu, Y. Qiao, H. Li, J. Dai, and W. Wang, "Vision-rwkv: Efficient and scalable visual perception with rwkv-like architectures," *arXiv preprint arXiv:2403.02308*, 2024.
- [36] D. P. Kingma and J. Ba, "Adam: A method for stochastic optimization," *arXiv preprint arXiv:1412.6980*, 2014.
- [37] T. Xue, B. Chen, J. Wu, D. Wei, and W. T. Freeman, "Video enhancement with task-oriented flow," *International Journal of Computer Vision*, vol. 127, no. 8, pp. 1106–1125, 2019.
- [38] R. Mantiuk, K. J. Kim, A. G. Rempel, and W. Heidrich, "Hdr-vdp-2: A calibrated visual metric for visibility and quality predictions in all luminance conditions," *ACM Transactions on graphics (TOG)*, vol. 30, no. 4, pp. 1–14, 2011.
- [39] S. Tel, Z. Wu, Y. Zhang, B. Heyrman, C. Demonceaux, R. Timofte, and D. Ghinac, "Alignment-free hdr deghosting with semantics consistent transformer," in *2023 IEEE/CVF International Conference on Computer Vision (ICCV)*. IEEE Computer Society, 2023, pp. 12790–12799.
- [40] B. Zheng, X. Pan, H. Zhang, X. Zhou, G. Slabaugh, C. Yan, and S. Yuan, "Domainplus: Cross transform domain learning towards high dynamic range imaging," in *Proceedings of the 30th ACM International Conference on Multimedia*, 2022, pp. 1954–1963.
- [41] X. Li, Z. Ni, and W. Yang, "Afunet: Cross-iterative alignment-fusion synergy for hdr reconstruction via deep unfolding paradigm," *arXiv preprint arXiv:2506.23537*, 2025.